Estimation of cold pool areas and chilling hours through satellite-derived surface temperatures

M. A. Jiménez(a)[1] , A. Ruiz(b) and J. Cuxart(b)

(a) Department of Global Change Research, Institut Mediterrani d'Estudis Avançats (UIB-CSIC), Esporles, Illes Balears, Spain

(b) Grup de Meteorologia, Departament de Física, Universitat de les Illes Balears, Palma de Mallorca, Illes Balears, Spain

Abstract

A methodology is proposed to identify the coldest areas of the island of Mallorca through satellite-derived surface temperatures. Land-surface temperatures from the Meteosat Second Generation (MSG-LST) just before sunrise for 1 year starting on September 1, 2007, were used. Fields for situations with clear skies and weak wind nights were selected, corresponding to 173 days of the year under study. Under these conditions, cold pools were generated in the centre of the three main basins of the island, in agreement with previous numerical and climatological studies. Maps of minimum air temperature and chilling hours, averaged over a season or annually, were obtained from the MSG-LST fields. These maps were then associated with the requirements of actual crop distributions.

HIGHLIGHTS

1. **Cold pool regions were identified using satellite-derived temperatures.**
2. **Suitable regions for growing vegetables and fruit trees were found using the CH map.**

[1]IMEDEA (UIB-CSIC), Miquel Marquès, 21, 07190 Esporles (Illes Balears) Spain. E-mail: majimenez@imedea.uib-csic.es

3. The types of crops were evaluated using the CH map.

4. The methodology can be used in regions with poor observation density.

KEYWORDS: Chilling hours, cold pool, land-surface temperature, MODIS, Meteosat Second Generation, satellite-derived products.

1 Introduction

Clear nights with weak synoptic winds favour the development of local circulations, including down-slope and down-valley flows, land-sea outflows, and formation of cold pools (CPs) in the lower parts of basins and valleys, especially in local terrain depressions. Air temperature decreases markedly from before sunset to about midnight, after which the rate of cooling slows greatly (as described in Martínez et al. [2010]). Under these conditions, it is reasonable to assume that the minimum temperature of the night occurs close to sunrise, because even if it has occurred sometime before, the differences in value are usually small.

Monitoring the temporal and spatial evolution of the slope and valley flows and of the CPs is difficult using data solely from the observational network because the stations are few and often fail to capture the wide spatial variability of nocturnal structures. Nevertheless, they are the only source of good-quality data for comparison with other methods such as satellite information or the outputs of numerical models. Therefore, advances in the combined use of all these sources are needed to provide a comprehensive view of the phenomena under study. Of particular importance are methods that provide information on spatial structures and their evolution, controlling their quality by means of independent ground observations.

CPs can be very extensive in the bottom of wide basins, as in Utah [Clements et al., 2003] or along the Duero River [Martínez et al., 2010] and the Ebro River [Cuxart and Jiménez, 2012] in the Iberian Peninsula. However, local depressions where cold air accumulates and cools radiatively occur almost everywhere as long as the overall wind is weak and the skies are clear [Vosper and Brown, 2008]. In these areas, which can be of the order of metres to kilometres, the calm air emits longwave radiation into space, generating a strong surface thermal inversion (e.g., Geiger [1965]) that makes it difficult for the warmer air above to penetrate and warm it [Stull, 1988]. Therefore, to compensate for the heat loss, heat must come from the surface by water condensation or from the soil by heat conduction. If the CP is large, slope flows bringing in warm air may have an effect through episodic turbulent mixing.

In many parts of the world, the minimal temperatures in a region occur inside cold pools because the lack of ventilation allows the same mass of air to cool continuously during the night, as for example in the Peter Sinks basin [Clements et al., 2003], which holds the extreme minimum temperature record for Utah [Pope and Brough, 1996]. For deep cold pools, sometimes the weak solar heating in the short winter days is not enough to destroy the temperature inversion, making the CP event an episode lasting for several days, usually until a change of weather pattern occurs. In such cases, accumulation of pollutants [Allwine et al., 1992] and formation of frost and fog are common (for instance in the Ebro River valley Cuxart and Jiménez [2012] or on the island of Mallorca Cuxart and Guijarro [2010]), with important consequences for human health, transportation (reduced visibility), and crop production. Topographically induced CPs have been studied with experimental field campaigns [Clements et al., 2003] and using numerical modelling (two-dimensional as in Vosper and Brown [2008]; high-resolution mesoscale simulations as in Cuxart et al. [2007]) or satellite-derived temperatures (Martínez et al. [2010]; Cuxart et al. [2012]).

The first focus of this work is to study the CPs that form in the lower parts of the main basins of the island of Mallorca, as described in Cuxart and Jiménez [2007] from mesoscale modelling, especially their strength and spatial extent. Most of the crops grown on Mallorca are produced in these CP areas and are exposed to low temperatures that may condition their development, either putting the plants or their fruits at risk by frost, or furnishing the required number of chilling hours for timely growth of buds in spring. This research has explored which areas of the basins are the coldest and has tried to quantify the suitable extent for several selected crops of economic interest.

Many plants need a certain amount of time under cold temperatures, especially during winter dormancy, when buds and seeds are unable to grow mainly due to hormonal factors [DennisJr, 1994]. Karssen and Groot [1987] reported that a lack of abscisic acid or gibberellin acid induced weak or extra-deep dormancy respectively. Plants use winter dormancy to avoid cold-weather damage [Saure, 1985]. To enable good plant development in spring and progression to the bud-burst phase, sufficient exposure to cold winter temperatures is required in a process known as vernalisation or chilling. One way to quantify whether dormancy has been long enough is through the use of chilling hours (CH), a parameter that counts the number of hours below a certain temperature threshold during the cold period of the year. The number of chilling hours that each plant needs depends on the species. Too few CHs can cause sporadic and light bud break, poor fruit development, small fruit size, and uneven ripening times (Saure [1985]; Voller [1986]; Oukabli et al. [2003]).

On the other hand, plants are viable only in a certain temperature range, as noted for wheat crops in Porter and Gawith [1999]. The *lethal* temperatures are the maximum and minimum temperatures that the plant can endure, whereas the plant life cycle is well reproduced when the ambient temperatures are within the *optimal* temperature range. A plant stops growing when the ambient temperature is lower than the minimum growth temperature (MGT) over a certain period (a day, several months, or during a season), a value which is different for each variety of plant within a given species. It is possible to quantify these temperature thresholds through statistical techniques using in-situ temperature observations [Liu et al., 1998] or laboratory experiments [Bonhomme et al., 1994].

Because phenological models use cold accumulation as a predictor of bud burst, it is important to estimate properly the CHs that a plant experiences in a certain region [Cesaraccio et al., 2004]. In middle latitudes, with the vegetation rest period in winter and the active growing period in spring and summer, temperature is the key parameter for understanding plant phenology (Chmielewski and Rötzer [2002]; Jiménez et al. [2014]). However, there are no universal models that accurately predict the release of dormancy for a broad range of plant species and environmental conditions. Nevertheless, results from phenological models are crucial for growers and foresters to predict the onset of the growing season, to evaluate plant productivity, to select crop varieties for a specific region according to ambient conditions and to predict maturity dates, yields, and quality of crops, which improves market delivery.

CH are commonly computed from hourly temperature observations during a period of interest (typically 1 year or at least the coldest months of the year), counting the number of hours when the temperature is lower than a certain value. This temperature threshold is usually taken as 7 °C in temperate climates like the western Mediterranean Sea regions (Tabuenca [1972]; Egea et al. [2003]; Alburquerque et al. [2008]). However, this threshold may vary depending on the species, the climate, and the local ambient conditions of the region under study [González-Parrado et al., 2006]. Besides, CH can be computed from empirical formulations based on average (daily, monthly, or seasonal) air temperatures, as described in Elías and Castellví [2001] for the western Mediterranean Sea region. For continental climates, the Utah model [Richardson et al., 1974] is often used, whereas the Dynamic model (developed in the Jordan Valley, Israel, Erez and Couvillon [1987]; Fishman et al. [1987]) is normally used in more temperate climates [DennisJr, 2003]. Ruiz et al. [2007] and Alburquerque et al. [2008] found that the CH estimates obtained from the hours-below-7 °C model were better than those from the Utah and the Dynamic models for apricot and sweet cherry in the Mediterranean region.

Current methodologies for computing CH or MGT are based mainly on temperature observations at one single location. However, local effects, such as orography or vegetation cover, induce heterogeneities in the temperature fields and may cause significant temperature differences between nearby measurement points. As a result, the representativeness of an observation is reduced to a very small area close to the place where it was made. Building a map from sparse observations usually involves interpolation techniques that often ignore many features of the terrain, leading to incorrect values of CH and MGT in the maps.

Satellite-derived products have been extensively used to support agricultural applications.

For instance, Blum et al. [2013] estimated the canopy temperature of an olive orchard, and Fu et al. [2014] used satellite land-cover products to evaluate the performance of different phenological models in the Northern Hemisphere. In addition, Amorós-López et al. [2013] monitored the vegetation seasonal dynamics and land-cover and land-use changes of small- and medium-size crops, and Maselli et al. [2012] developed a methodology to predict the daily gross primary production of olive trees.

This work involved determining the coldest areas of the island of Mallorca using satellite-derived land-surface temperatures (LST), by means of the 1.5-m temperature of the surface stations as a quality-control parameter. Meteorological stations are scarce in the centre of the island, which is mainly devoted to agriculture. This situation does not permit accurate explicit spatial estimates of crop temperature requirements. With the proposed methodology, it is possible to derive maps of estimated minimum temperature, CH, and MGT from satellite LST fields.

2 Location and period of interest

Mallorca (Figure 1) is located in the western Mediterranean Sea and measures 70 km in the N–S and 100 km in the E–W directions. It has a mountain range on its north-western side (Serra de Tramuntana), with several peaks over 1000 m above sea level (asl), a discontinuous lower mountain range on its south-eastern side (Serra de Llevant), and an elevated area in the centre of the island. This topographical configuration results in three main basins: the Palma basin in the south-west, the Campos basin in the south, and the Alcúdia basin in the north-east. Crops in Mallorca are cultivated mainly in the low areas between mountain ranges [Ginard et al., 1998], which correspond to the basins just described.

Previous numerical studies on the island of Mallorca (Cuxart et al. [2007]; Jiménez et al. [2008]) showed that cold regions occur at night in the central areas of the three basins (see

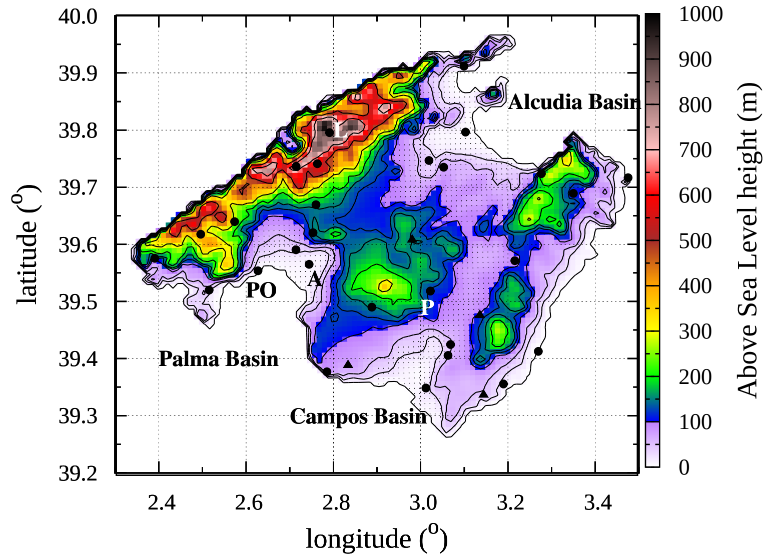

Figure 1: Topography of the island of Mallorca with surface stations from the AEMET network (in dots) and the OCLIB network (in triangles). Some selected locations are labelled as: *A*, the airport; *PO*, Portopí; *P*, Porreres; and *L*, Lluc. The central parts of the three main basins are coloured in purple, and their names are indicated over the sea, in front of the coastline. The shaded areas show the coldest nocturnal temperatures found in Cuxart et al. [2007] and Jiménez et al. [2008] for one clear-sky night.

shaded areas in Figure 1), where CPs are formed under clear sky and weak wind conditions. Nocturnal temperatures are also low in the narrow or closed valleys in the northern mountain range. Similar results were found by Cuxart and Guijarro [2010] using surface stations from the AEMET network (Spanish Meteorological Weather Service, indicated with dots in Figure 1) to compute climatological statistics from 1972 to 2008. They showed that the number of days of frost (temperatures lower than 0 °C) or cold (temperatures lower than 7 °C) decreased during the period under study. However, the spatial temperature patterns of Mallorca were mostly unchanged, and the coldest areas were always located in the centres of the basins and in the closed valleys in the northern mountain range.

A complete year from September 1, 2007 to August 31, 2008, has been analysed in this work. In Figure 2, the yearly evolution of the minimum temperature for the Airport station

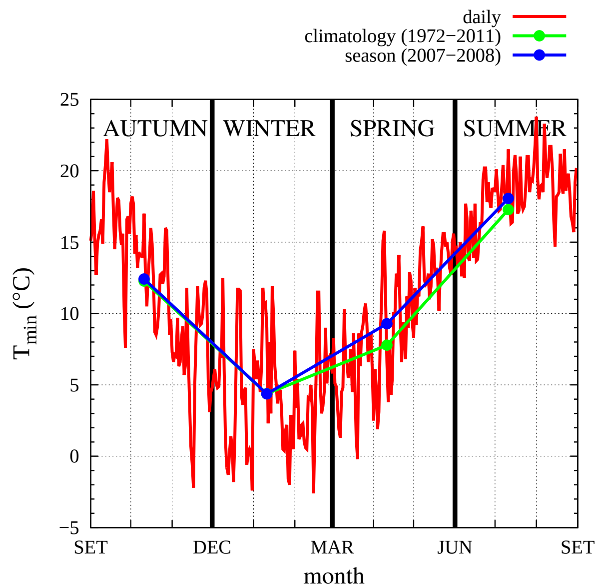

Figure 2: Evolution of the daily minimum temperature observed at the airport (see location in Figure 1), together with seasonal averages over the period of interest (September 2007–August 2008, blue line) and historical climate (1972–2011, green line).

(labelled as A in Figure 1) is shown, and the seasonal averages of that year are compared with the climatological values for 1972–2011. Values during autumn and winter are similar to the climatological values, whereas during spring and summer 2008, they are slightly warmer. The units of temperature throughout the manuscript are °C. The accumulated rainfall (525 mm, 2007–2008) was greater than the 30-year mean (424 mm, 1970–2000) due to the rainy autumn and spring seasons.

3 Satellite-Derived Land-Surface Temperatures

Data from Meteosat Second Generation (MSG; Schmetz et al. [2002]), a geostationary satellite launched in 2002 by the European Organisation for the Exploitation of Meteorological Satellites (EUMETSAT), were used in this research. The Spinning Enhanced Visible and Infrared Imager (SEVIRI) on board MSG provides measurements in 12 spectral channels, every 15 min, and with a spatial resolution of about 25 km^2 per pixel in the area of interest. After radiometric and geometric corrections [Schmetz et al., 2002], the land surface temperature (LST) can be estimated directly from channel 9 (10.8 μm). Note that channel 9 surface brightness temperatures are on average 1–2 °C colder (depending on ambient conditions, wind, and soil humidity, among other factors) than those observed at the surface [Coll et al., 1994] because the correction for the atmospheric water vapour effect has not been applied. To apply this correction, information about the thermal and water vapour vertical structure of the atmosphere is needed, and MSG does not provide this information. Therefore, the corresponding bias is present in the MSG-LST fields used in this work.

Unlike MSG-LST, the LST derived from the MODerate resolution Imaging Spectroradiometer (MODIS, Salomonson et al. [1989]) are corrected for the effect of atmospheric water vapour. MODIS is on board the polar Aqua and Terra satellites, which are equipped with instruments that can estimate the atmospheric temperature and water vapour column-integrated values that are used to correct the MODIS-LST fields for atmospheric effects [Wan and Dozier, 1996]. These polar satellites orbit at a distance of 705 km above the Earth's surface, much closer than MSG which is geostationary at 36000 km, providing high horizontal resolutions (about 1 km^2). However, MSG provides one LST field every 15 min, whereas there are at most 4 MODIS-LST fields per day. Therefore, MSG-LST fields will be used as the main data input because they have already proven their utility for detecting CPs on Mallorca [Jiménez et al., 2008].

3.1 Estimation of air temperatures from LST

To account for the bias between the observed surface and 1.5 m (above the ground) temperatures a linear regression between the MSG-LST fields and the observations from surface weather stations was performed. The value of the closest MSG-LST pixel to each surface weather station was compared to the air temperature observed at the weather station. Here, a linear regression is provided between LST and minimum air temperatures, assuming that these take place just before sunrise for a selected subset of days. All the observations were taken from official networks (AEMET and OCLIB, Balearic Islands meteorological network) except for those surface weather stations situated in very complex terrain (in small terrain features in the valleys or on peaks in the northern and eastern mountain ranges), where the value of the MSG-LST pixel is not comparable with the observation.

3.2 Minimum satellite-derived LST

As mentioned before, it has been assumed that in flat terrain and homogeneous areas under clear sky and weak wind conditions, the minimum air temperature occurs close to sunrise. In more complex terrain regions, basin- or local-scale advections can occur (such as down-slope winds [Cuxart et al., 2007]), producing mixing events that might reduce the nocturnal cooling rate and even increase the temperature for some period of time during the night [Vich et al., 2007]. As in most pollutant dispersion studies [Sharan et al., 1996], it will be defined that weak wind conditions exist when 2 m winds are less than 2 m s^{-1}, which corresponds to 10 m winds of less than 4.4 m s^{-1}. This value is found if the Businger-Dyer relations are used (Businger et al. [1971]; Dyer [1974]), assuming that wind speed decreases logarithmically with height and that typical scales under night-time conditions of roughness length (0.1 m), friction velocity (0.2 m s^{-1}), and surface heat flux (0.01 K m s^{-1}) are used.

As mentioned, the last MSG-LST field before sunrise was selected, assuming that this hour is when the minimum air temperature occurs. This assumption was checked between September 2007 and August 2008 for pixels close to the surface weather stations on the island (see locations in Figure 1), and it was found to be correct for 69% of days (72% for inland stations) and for most days with clear skies and weak winds (91%).

To select the satellite images, the following criteria were used:

1. MSG-LST fields were obtained only under clear sky conditions. Therefore, when clouds

were present, the MSG-LST values of these pixels were void. Only cases when more than 50% of the points for Mallorca had non-void MSG-LST values were accepted. These corresponded to 58% of the days within the study period. Figure 3a shows the time series of the percentage of pixels for Mallorca with non-void MSG-LST; the black points correspond to the days eliminated according to this criterion (0% means that all the pixels over Mallorca have void values).

2. In cases of moderate to strong winds, the minimum temperature can happen at a time not near sunrise. To guarantee that the selected days had a minimum temperature close to sunrise, a filter was used to eliminate non-weak wind cases. The daily wind run (calculated by multiplying the wind speed by the measurement interval and integrating over 1 day) at the airport during the period of interest is shown in Figure 3b. It was found that from September 2007 to August 2008, the average wind run was (256±104) km day^{-1}. Days with a wind run greater than 400 km day^{-1} (corresponding to a daily mean value of 4.4 m s^{-1}) that fulfilled criterion (1) were eliminated (20 days, indicated by green asterisks in Figure 3). The wind run of most days that fulfilled conditions (1) and (2) was between 100 and 300 km (corresponding to mean winds of 1–3.4 m s^{-1}).

3. The presence of water on the surface (related to a previous rain event) might also alter the satellite-derived surface temperature due to changes in surface emissivity associated with the increase in surface wetness. To avoid this problem, the days after a rain event were also eliminated (a total of 18 days, Figure 3).

The set of selected days represents 47% of the days of the year (see red dots in Figure 3), of which 91% had the minimum temperature close to sunrise as indicated in the airport observations. For the remaining 9% of days, the minimum temperature took place sometime in the three hours before sunrise. During these days, down-slope flows may have interrupted nocturnal cooling due to associated enhanced mixing by turbulence with warmer air from

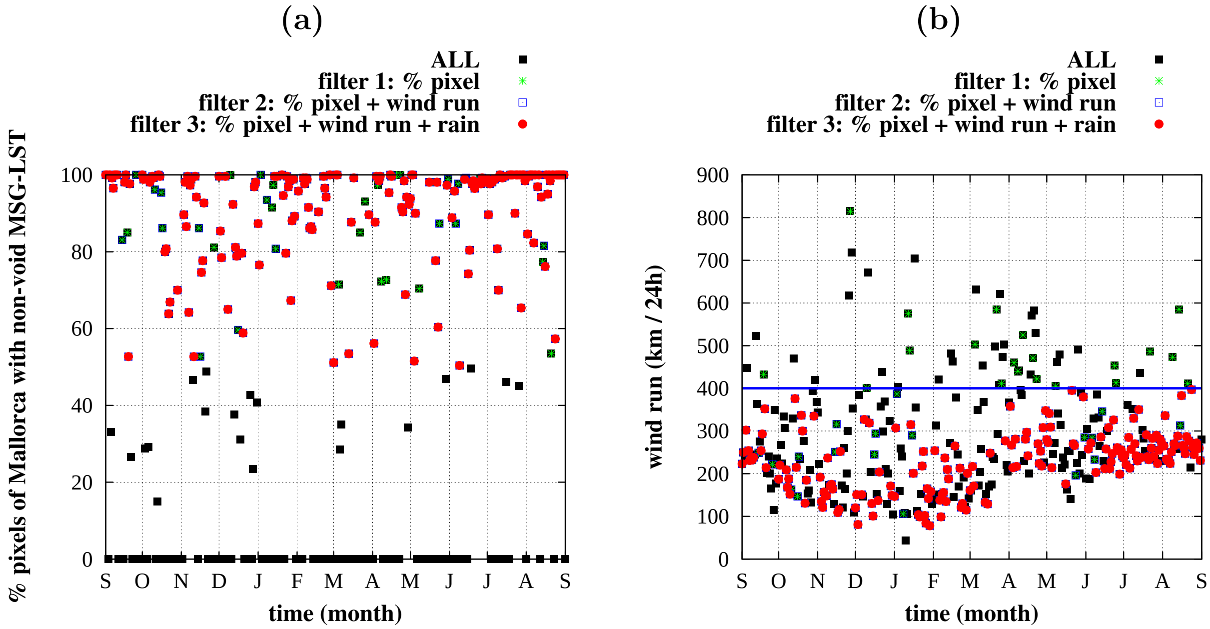

Figure 3: **(a)** Percentage of points in Mallorca with non-void MSG-LST values over the period of interest (September 2007–August 2008). The days that fulfilled the criteria explained in the text are shown in different colours, and those fulfilling all the filters (corresponding to weak wind and clear sky conditions) are shown in red. **(b)** Time series of the daily wind run (in km day^{-1}) at the airport over the period of interest. The value of 400 km day^{-1} was taken as a threshold value (criterion 2) and is indicated in the plot by a blue line.

above [Martínez and Cuxart, 2009].

Inspection of the surface maps† indicated that during the 173 selected days that fulfilled the filtering criteria, Mallorca was under the influence of high-pressure systems (especially during summer) or in an area of weak pressure-gradient conditions. As has been shown by Jiménez et al. [2008], under these conditions, the coldest temperatures occur in CP areas, where there is a surface temperature inversion. For most of the other 193 nights, CP formation might be absent, and the areas with the lowest temperatures on the island could be found in the Tramuntana mountain range.

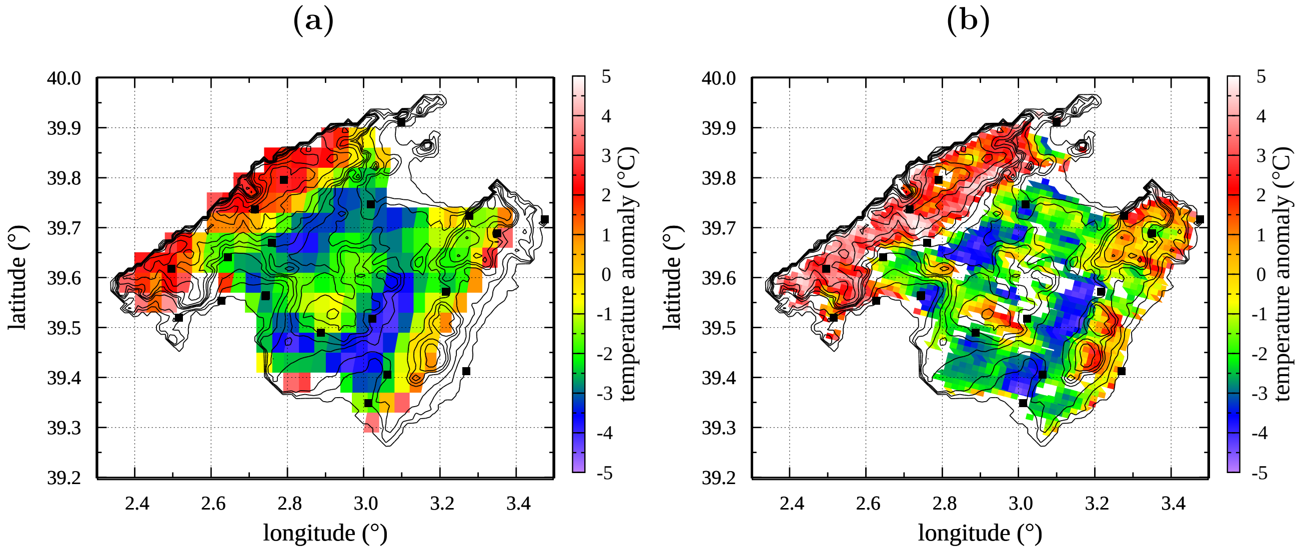

Figure 4: Land surface temperature anomalies on January 29, 2008, at 0200 UTC computed from **(a)** MSG-LST and **(b)** MODIS-LST. The topographic lines are included, and AEMET surface weather stations are indicated with dots.

3.3 Validation of the MSG-LST

To identify the location of the coldest areas in Mallorca, the temperature anomalies with respect to the island mean value (computed as LST-<LST>, where LST is the satellite-derived surface temperature at one grid point and <LST> is the mean temperature of all the grid points on the island), were calculated and are shown in Figure 4 for a particular night (January 29, 2008, at 0200 UTC). A MODIS image is also available that makes it possible to compare the anomalies seen by both satellites.

In Figure 4, similar patterns in the temperature anomaly fields can be seen for both satellites. MODIS has a finer spatial resolution and describes the land-sea discontinuity better. Due to the lack of atmospheric correction, the MSG-LST mean temperature of all the grid points on the island (5.6 °C) is warmer than that computed from the MODIS-LST fields (4.2 °C), but within the ranges (1–2 °C) found by Coll et al. [1994].

For the entire study period, and for the subset of nights of interest, available MODIS-LST

†available from http://www.wetterzentrale.de/topkarten/fsreaeur.html

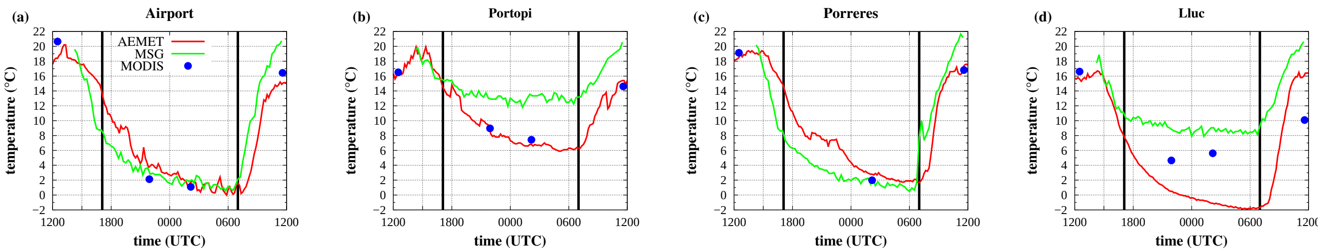

Figure 5: Time series of the observed 1.5 m temperature (red lines) and the land-surface temperature derived from MSG (green lines) and MODIS (in dots) from January 28, 2008, at 1200 until noon of the next day for several locations: **(a)** the airport, close to the coast, 7 km inland; **(b)** Portopí, on the coast; **(c)** Porreres, in the centre of the Campos basin, and **(d)** Lluc, inside a closed valley in the northern mountain range. The vertical black lines indicate the sunrise and sunset hours.

and MSG-LST reproduced the same patterns when compared. The anomalies show that the coldest areas are located in the centre of the three basins, where CPs are formed, with values of about 4 °C below the mean LST of the island. On the other hand, the warmest regions (anomalies of approximately 2 °C) correspond to the mountain ranges in the northern and eastern parts of the island and the elevated area between them. Near the coast, the MSG-LST fields do not have enough spatial resolution to capture coastal irregularities, with the result that points on the coastline are mainly considered as sea points instead of land points.

The impact of topographical features at the subpixel scale on the MSG-LST fields can be seen in Figure 5. The temporal evolution (24 hours starting on January 28 at 1200 UTC) of MSG-LST at four locations (indicated in Figure 1) shows trends similar to the 1.5 m temperature at the surface station and to MODIS-LST. These three sources of temperature reproduce the same temporal evolution in the inland stations (Airport and Porreres, Figure 5), which have relatively homogeneous terrain at the subpixel scale. On the coast (Portopí, Figure 5b), MODIS-LST and 1.5 m temperature behave similarly, but are colder than the MSG-LST due to the larger amount of sea in the pixel for MSG and the lack of atmospheric correction. The spatial resolution and the lack of atmospheric correction can also explain the bias between the satellite-derived temperatures from both satellites inside a small closed mountain valley (Lluc, Figure 5d). Here, both LST sources are unable to reproduce the observed strong nocturnal cooling, and the satellite LSTs are about 10 °C warmer than those observed at 1.5 m by the surface station.

For inland areas with low surface heterogeneity, where basin CPs develop, both satellites provide similar values and patterns for the LST, despite the consistent cold bias related to the lack of atmospheric correction for MSG, and with temporal trends very similar to the 1.5 m air temperatures. MSG-LST fields near sunrise were used for the analysis because they are available every 15 min and enable the generation of LST time series and spatial maps.

3.4 Seasonal average minimum LST anomaly

Figure 6 shows a map of the average MSG-LST anomalies just before sunrise for the subset of selected clear nights with non-strong winds for winter, summer, and autumn (similar in temperature patterns to spring, not shown), separately and for the whole year. The cold anomalies in the centre of the basins are clearly seen in winter and autumn, with values of -3 °C (spring, not shown, had similar patterns, with values of -2 °C). In summer, the cold anomaly is maximum in the central area of the island, and the basins are still colder than the island average, implying less accumulation of cold air in the centre of the basins due to shorter nights and very warm conditions at sunset. The annual average anomalies showed a pattern very similar to that observed in winter, with values in the basins of about -2 °C, in agreement with the climatological analysis of Cuxart and Guijarro [2010]. Therefore, except for summer nights, it can be concluded that the cold patterns in the lower parts of the basins are a distinct feature of the climate of the island.

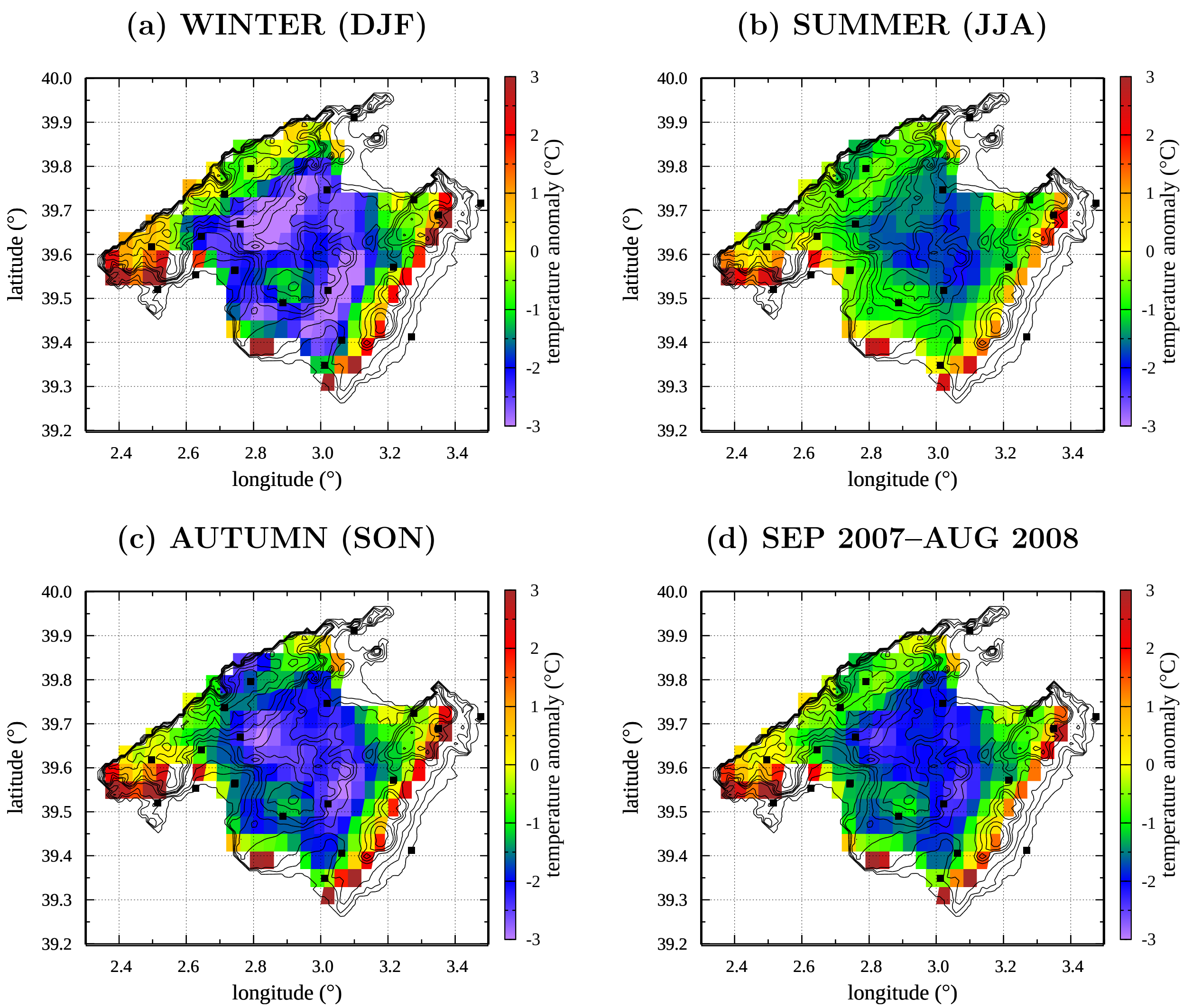

Figure 6: Average minimum temperature anomalies over different periods: **(a)** winter (DJF); **(b)** summer (JJA); **(c)** autumn (SON), and **(d)** annual (1 year starting on September 1, 2007). Only the days that satisfied the filter conditions (clear skies and weak wind conditions, see further explanation in Section 3.2) have been considered in these averages.

3.5 Estimation of Chilling Hours

The number of CHs was estimated by counting the number of hours when the temperature was below 7°C for certain selected stations using the available hourly data, at the coast, in the mountains, and inland (Table 1; see locations in Figure 1).

Table 1: Chilling hours (CH) computed from hourly temperature observations during September 2007–August 2008 and averaged over three different regions: coastal, mountain, and inland. The mean bias was computed as $\sum_i (CHF_i - CHO_i)$, where the i are all the stations in each region and CHF_i and CHO_i are respectively the computed and observed CH (hours when the temperature is less than 7 °C).

	method	coastal	mountain	inland
number of stations		6	2	6
$< CH > \pm\sigma$	hours when T< 7 ° C	214±167	1316±71	589±161
mean bias	satellite-derived (Equation 2)	-134	(*)	60

(*) Equation 2 is not valid for mountain regions.

Different formulations developed for the western Mediterranean Sea regions show that CH can be computed using solely the minimum air temperatures during winter [Elías and Castellví, 2001]. A linear regression will be derived between these two variables that will be used in the construction of a CH map for the central part of the island, using also the regression previously found between MSG-LST and 1.5-m temperature described in Subsection 3.1. The performance of this method will be assessed using the mean bias for all the stations in each region as $\sum_i (CHF_i - CHO_i)$, where i are all the stations in each region and CHF_i and CHO_i are respectively the CH estimated with the proposed formulation and those computed counting hours below 7 °C.

4 Results

4.1 Estimation of daily minimum air temperatures

Using the linear fit (Figure 7a) of the observed minimum 1.5 m temperatures and the MSG-LST values at the nearest grid point, it was found that:

$$T_{1.5m} = (0.86 \pm 0.01) \times T_{sat} + (1.35 \pm 0.14) \quad (1)$$

where $r^2 = 0.75$ with a level of significance $p < 0.0001$. The uncertainties in Equation 1 are provided by the standard deviation of the regression coefficients. The error of the estimated $T_{1.5m}$ from the linear fit (Equation 1) is 3.21 °C, computed from the standard error of the estimate (sum of squared differences between the actual scores and the predicted scores) and divided by the number of pairs ($T_{1.5m}$, T_{sat}). This error is related to the warm bias of the MSG-LST fields, which is not uniform for all points over the island. Besides, for stations close to the coast, the MSG-LST values are strongly influenced by the warm sea-surface temperature. In Figure 7a, measurements at one single point ($T_{1.5m}$) are compared to averages over an area of 25 km^2 (T_{sat}), and the representativeness of the surface station can be low, especially in heterogeneous regions (due to orography or soil cover). The impact of the $T_{1.5m}$ error on the computation of CH will be explained in the next section.

By applying Equation 1 to the LST-MSG fields, maps of average minimum air temperatures have been built (Figures 7b and 7c). These average temperature maps are similar to those obtained by Cuxart et al. [2007] for a selected case through high-resolution mesoscale modelling.

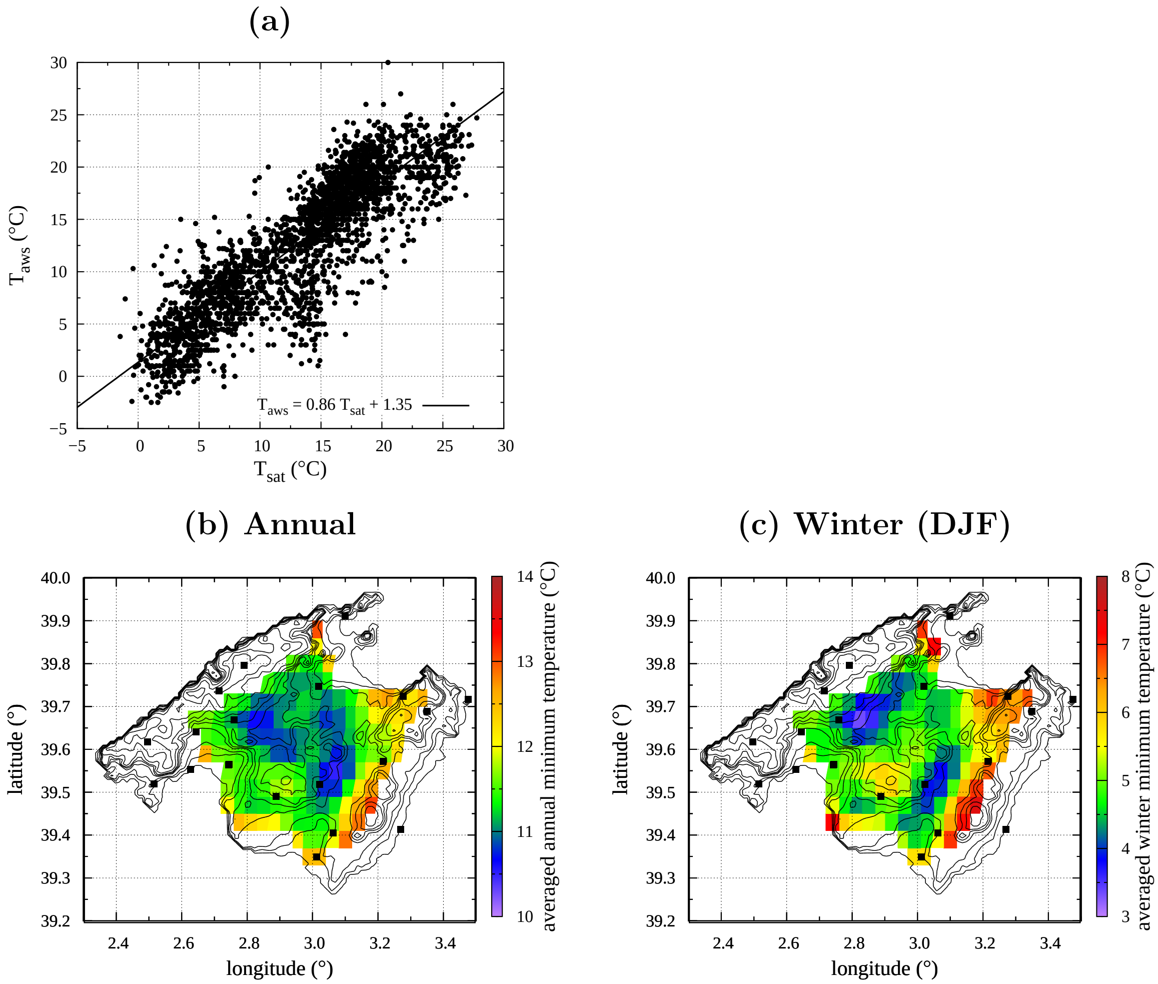

Figure 7: **(a)** Linear regression of the observed 1.5-m air temperatures and those obtained from MSG considering all the surface stations represented in Figure 1 from the AEMET and OCLIB networks, except those in the mountain regions. **(b)** Annual minimum air-temperature map computed from the linear fit in **(a)** and the average annual MSG-LST (Figure 6d). The same occurs in **(c)** for the winter minimum air temperature. Only the days that fulfil the filter conditions (clear skies and weak wind conditions, see further explanation in Section 3.2) have been considered in the linear fit and in the averages.

4.2 Computing CH from surface weather stations

Figure 8 shows the relation between the observed CH during the year analysed and the average of the daily minimum air temperature during winter, considering all the days (not only those satisfying the filter conditions explained in Section 3.2). From the linear fit (Figure 8), it was determined that

$$CH = (-111.6 \pm 13.5) \times < T_{min} >_{winter} + (1150.1 \pm 94.8) \tag{2}$$

where $r^2 = 0.872$ and the level of significance $p < 0.0001$. The error of the estimated CH from Equation 2 is 97.4 hours, but it increases to 145 hours using the error propagation method and the uncertainty of the surface temperature (obtained from the linear fit in Equation 1).

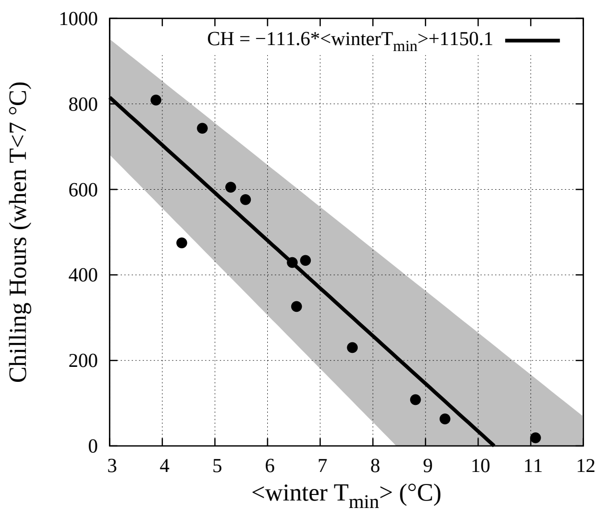

Figure 8: Correlation between average winter minimum temperatures and chilling hours for the surface stations of the AEMET network (except for those in the mountains). The grey area indicates the mean values and the standard deviation of the linear fit.

All stations were used except those inside narrow mountain valleys; including these diminishes the correlation to $r^2 = 0.672$. Stations located at high altitudes have average minimum temperatures of about 4 °C and CH close to 1000, essentially due to the decrease

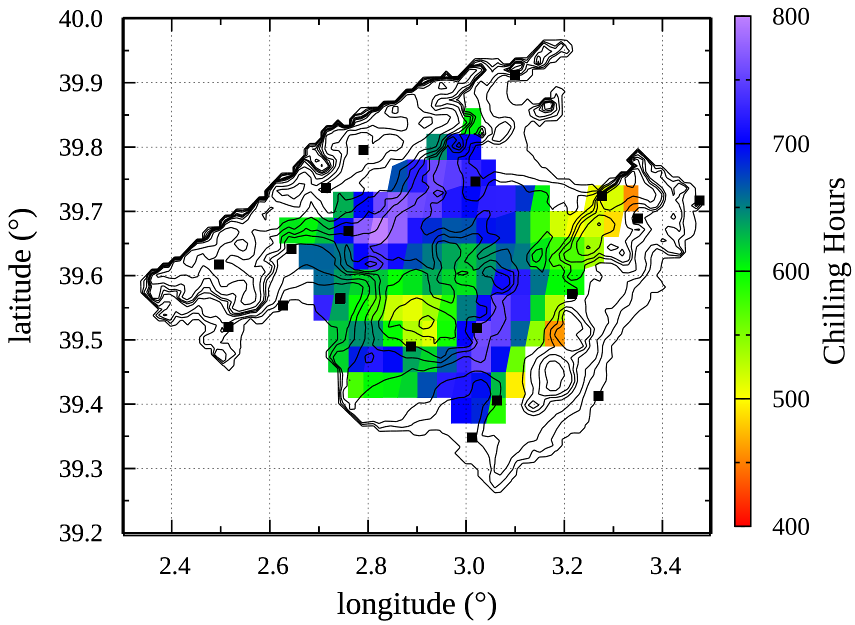

Figure 9: Chilling hours computed from the linear fit (Equation 2) and the winter minimum temperatures derived from the MSG-LST in Figure 7c (mountain regions excluded).

of temperature with height, because high-altitude stations in CP-prone areas were removed from the analysis. Because the flatland's winter minimum temperatures are between 2 and 5 °C, linear regression shows that for these areas, the value of CH is greater than 500 on average.

The linear fit obtained from Equation 2 was applied to the average minimum air temperatures during winter (shown in Figure 7c). Figure 9 shows a CH map for the whole island, excluding the mountain regions. The largest number of CHs are found in the regions where CPs are generated (Figure 7c).

The bias between the CHs computed from Equation 2 and those directly counted from the hourly temperatures is shown in Table 1. For the coastal stations, the estimated CHs were less than those computed from measurements (negative bias) due to the contribution to these pixels of warm sea areas. For the inland stations, the difference between the estimates and the directly computed values was significantly reduced. This good correspondence comes from the fact that Equation 2 was derived using observations from Mallorca, and therefore it will only be valid for computing CH there. This is a common characteristic of other formulations (as in Elías and Castellví [2001]), which have been documented to work well for the regions where they were produced, but have large biases (not shown) for the data set used in this research.

The methodology proposed here provides good estimates of minimum air temperature patterns (similar to those found in Cuxart and Jiménez [2007] from mesoscale modelling), especially for inland regions where the sources of error in the MSG-LST fields are fewer (land/sea mask, pixel heterogeneity, and surface emissivity). In these areas, the network of observations is not very dense, and the estimated CH has an error of at most approximately 15%. Although the results were derived for weak winds and clear sky conditions in the central part of the island, the CH computed using surface observations for the filtered days was similar to those computed using all days.

5 Applications to agriculture

This section describes the application of the CH and minimum air-temperature maps obtained in the previous section to the needs of agriculture in Mallorca.

5.1 Best places to cultivate based on CH requirements

The CH requirements for some fruits and nuts grown in Mallorca, together with the area currently occupied and the amount of production, are shown in Table 2. It is seen that most of the cultivated areas in Mallorca are devoted to almond trees and grapes (vineyards). The atlas of the Balearic Islands [Ginard et al., 1998]† shows that almond trees are very common

†http://www.uib.cat/secc6/lsig/Atles/INICI.HTM

Table 2: Fruits and nuts grown in Mallorca with the required CH (maximum and minimum) extracted from Gil-Albert [1986] and Elías and Castellví [2001] for crops in the Iberian Peninsula. Area occupied and production are for 2009 for the Balearic Islands, but more than 90% of these values also correspond to Mallorca [Estadistiques Illes Balears, 2009] .

	CH_{min}	CH_{max}	Extent (Ha)	Production (10^3 kg)
almond	100	500	24443	1358
grape	100–500	1400	1795	5932
apple	200–800	1700	101	1168
apricot	200–500	900	425	396
pear	500	1000	28	229
peach	100–400	1100	124	170
plum	700	1600	134	98
nuts	400	1500	6	31
cherry	500–800	1500	29	18
hazelnut	800	1600	(*)	(*)
raspberry	800	1600	(*)	(*)

(*) only grown in some valleys in the northern mountain range, but not for commercial purposes.

in the central, southern, and eastern regions of Mallorca, especially in the Campos basin, but are not grown in the northern mountain range. Most dense almond tree regions are within the limits of CH (Table 2 and Figure 8b), but almond trees are also found in places where the CH are above this limit.

CH requirements are less restrictive for vineyards, which can be grown on almost the entire island. However, they are grown only in some regions in the centre of the island [Ginard et al., 1998], located where the CHs are greater than 650 in Figure 8b. An important piece of information that the CH map of Mallorca is offering to the farmers is that, in terms of cold temperature requirements, grape production could be increased in the future by devoting more area to this crop. The CH map could be of use in evaluating regions for expansion of already existing crops and to explore the possibility of introducing new ones. This information could not be obtained from classical methods in which the CHs are computed using temperature observations from a surface weather station at one single location.

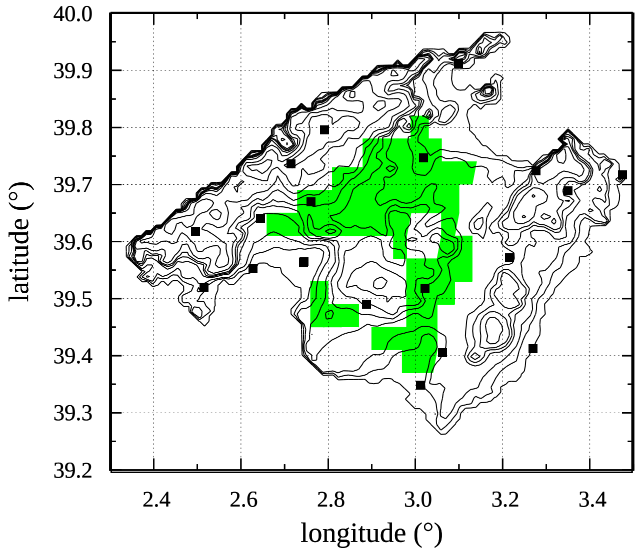

Figure 10: Regions with CH between 200 and 500 hours where it is appropriate to cultivate apricots, according to the chilling hours requirements (Table 2 and Figure 8b).

The apricot is a case of a fruit that is mainly grown in the centre of Mallorca and that has significant requirements in terms of CH. The agricultural cooperative in Porreres† (see location in Figure 1) grows 80% of Mallorca's production. According to Table 2 and the map in Figure 8b, the most suitable regions to cultivate apricots are shown in Figure 10 and are located essentially in the central part of the island, specifically the Campos basin, where most existing production is located. However, ambient conditions are also favourable in other regions in the central part of the island, where production is currently low.

5.2 Best places to cultivate based on minimum growth temperature requirements

Some of the crops cultivated in Mallorca do not have MGT requirements, but for some others, knowledge of this value is crucial to evaluate crop yield (Table 3).

†http://www.cooperativa-agricola-porreres.com/

Table 3: Minimum growth temperature (MGT) for different crops in Mallorca, together with the temporal interval over which this minimum has to occur according to Elías and Castellví [2001] for crops in the Iberian Peninsula. The extent and production of these crops for 2009 in the Balearic Islands is also included. [Estadistiques Illes Balears, 2009].

name	MGT (°C)	period [initial , final]	Extent (Ha)	Production (10^3 kg)
barley	6	[March (or July), May (or September)]	21842	73522
lima beans	6–12	[October, March]	1727	1363
peas	5–7	[October–February, February–June]	501	437
potatoes	5	[April , October]	1542	54230
tomatoes	8	[April , October]	242	11140
watermelon	11	[March 15, August 30]	329	11347
onions	6	[September 1, March 15]	298	8864
lettuce	5	[October 1, March 30]	290	7972
melons	8	[April 1, September 30]	147	3847
zucchinis	10–15	[August–December, October–February]	141	2394
artichokes	7	[July 1, May 1]	41	476

Here, tomatoes will be taken as an application illustration (Table 3). It is known that the MGT is 8 °C from April to October. From the monthly average minimum temperature maps obtained in Section 3 using MSG-LST, April is the only month of the period from April to October for which the minimum temperature can be lower than the MGT. Figure 11 shows the number of days in April 2008 with a daily minimum temperature lower than the MGT. Temperatures lower than the MGT are more frequent in the coldest areas of the central part of the island than in the other regions. Tomatoes are already grown mainly in these regions [Estadistiques Illes Balears, 2009], and typically they are protected during April and May to prevent the plant from experiencing temperatures below the MGT and to guarantee successful production. Similar protective techniques, such as shading screens [Teitel et al., 1996], are used in fields of other crops (see Table 3).

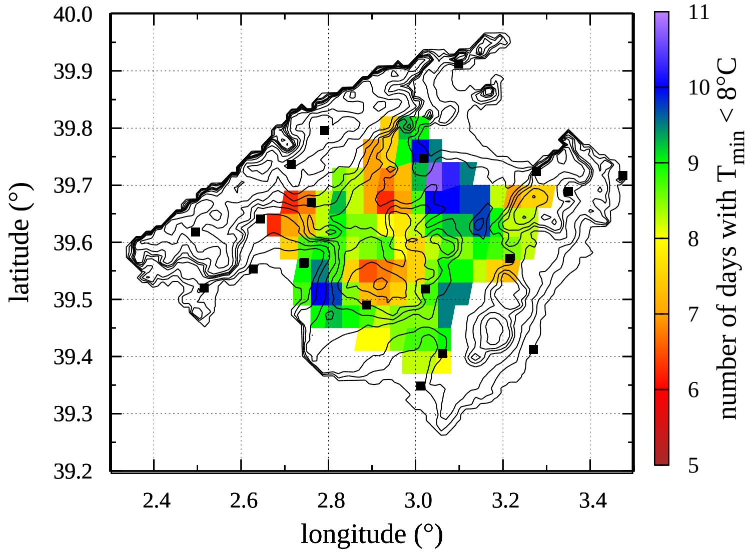

Figure 11: Number of days in April 2008 with a minimum temperature lower than 8 °C (minimum growth temperature for tomato, Table 3).

6 Conclusions

From the analysis of satellite-derived surface temperatures under clear sky and weak wind conditions for 1 year, the coldest areas in Mallorca have been located in the centre of the three main basins of the island, in agreement with the results of previous studies using mesoscale modelling (Cuxart et al. [2007]; Jiménez et al. [2008]). Cold pools occur where cold air is formed locally and further accumulated by down-slope winds.

The methodology proposed here shows a good correspondence between satellite-derived temperatures and air temperatures under the conditions described above. The sources of the errors in derived air temperature include subpixel heterogeneity-including the sea-land limit, the variations in surface emissivity during the day which were not accounted for, and the failure to correct for the effect of atmospheric water vapour.

The network of observations is not dense on the island, and this method makes it possible to identify cold regions under clear sky and weak wind conditions. This information may be of use for agricultural purposes and as an input to phenological models, as indicated in the following points.

1. Typically, chilling hours are derived using temperature observations at one point. The main advantage of the proposed methodology is that it is possible to build a chilling-hour map using satellite-derived temperatures, provided that the uncertainty is given.

2. The chilling-hour maps are useful in identifying the best locations to grow a crop (in terms of the requirement for cold conditions) to guarantee a successful yield.

3. The minimum growth temperature maps that can be built with the proposed methodology are also important in evaluating the periods when protective measures are needed to avoid placing the plant under extremely cold temperatures and making it stop growing.

4. The chilling-hour and minimum growth temperature maps can be used for decision-making support for crop planning in a given region.

The methodology can be easily extended to other mid-latitude regions (with similar temperature ranges along the annual cycle) where clear sky and weak wind conditions are frequent. The input requirements are first, to have available observations of air temperature (at least every hour) at several locations (not necessarily a dense network of surface observations) and second, to extract satellite-derived temperatures close to sunrise (from MSG or another geostationary satellite depending on the location of the region under study). Linear equations similar to Equation 2 obtained here must be computed for each location independently.

The more homogeneous the region, the better the results will be, because the satellite-derived temperatures under quasi-homogeneous conditions will be closer to the values observed by surface weather stations. The spatial resolution of the satellite-derived temperatures is also important because sub-pixel effects are misrepresented in coarser-resolution fields. Further work is needed to evaluate the quality of these fields in comparison to surface observations, and the representativeness of the area close to the surface weather station should be carefully examined.

Acknowledgements

The land surface temperatures derived from MSG were taken from the Land Surface Analysis Satellite Applications Facility (LSA-SAF) and the surface observations from the AEMET (Spanish Government) and OCLIB (Balearic Islands Government) networks. A. Lázaro is acknowledged for helping in computing some statistics. This work was funded through the projects CGL2009-12797-C03-01 and CGL2012-37416-C04-01 of the Spanish Government, supplied by the European Regional Development Fund (FEDER), and with a JAE-Doc contract from the *Junta para la Ampliación de Estudios* program from CSIC supplied by the European Social Fund.

References

N. Alburquerque, F. García-Montiel, A. Carrillo, and L. Burgos. Chilling and heat requirements of sweet cherry cultivars and the relationship between altitude and the probability of satisfying the chill requirements. *Environ. Exp. Bot.*, 64:162–170, 2008.

K. J. Allwine, B. K. Lamb, and R. Eskridge. Winter-time dispersion in a mountainous basin at Roanoke, Virginia: Tracer study. *J. Appl. Meteor.*, 31:1295–1311, 1992.

J. Amorós-López, L. Gómez-Chova, L. Alonso, L. Guanter, R. Zurita-Milla, J. Moreno, and

G. Camps-Valls. Multitemporal fusion of Landsat/TM and ENVISAT/MERIS for crop monitoring. *International Journal of Applied Earth Observation and Geoinformation*, 23: 132–141, 2013.

M. Blum, I. M. Lensky, and D. Nestel. Estimation of olive grove canopy temperature from MODIS thermal imagery is more accurate than interpolation from meteorological stations. *Agric. Forest. Meteorol*, 176:90–93, 2013.

R. Bonhomme, M. Derieux, and G.O. Edmeades. Flowering of diverse maize cultivars in relation to temperature and photoperiod in multilocation field trials. *Crop Sci.*, 34:156–164, 1994.

J.A. Businger, J.C. Wyngaard, I. Izumi, and F.E. Bradley. Flux-profile relationships in the atmospheric surface layer. *J. Atmos. Sci.*, 28:181–189, 1971.

C. Cesaraccio, D. Spano, R.L. Snyder, and P. Duce. Chilling and forcing model to predict bud-burst of crop and forest species. *Agricultural and Forest Meteorology*, 126:1–13, 2004.

F.-M. Chmielewski and T. Rötzer. Annual and spatial variability of the beginning of growing season in Europe in relation to air temperature changes. *Clim. Res.*, 19:257–264, 2002.

C. B. Clements, C. D. Whiteman, and J. D. Horel. Cold-air-pool structure and evolution in a mountain basin: Peter Sinks, Utah. *J. Appl. Meteorol.*, 42:752–768, 2003.

C. Coll, V. Caselles, J. A. Sobrino, and E. Valor. On the atmospheric dependence of the split-window equation for land surface temperature. *Int. J. Remote Sens.*, 15:105–122, 1994.

J. Cuxart and J. A. Guijarro. Observed trends in frost and hours of cold in Majorca. *Int. J. Climatol.*, 30:2358–2364, 2010.

J. Cuxart and M. A. Jiménez. Mixing processes in a nocturnal low-level jet: An les study. *J. Atmos. Sci.*, 64:1666–1679, 2007.

J. Cuxart and M. A. Jiménez. Deep radiation fog in a wide closed valley: study by numerical modeling and remote sensing. *Pure and Applied Geophysics*, 169:911–926, 2012.

J. Cuxart, M. A. Jiménez, and D. Martínez. Nocturnal meso-beta basin and katabatic flows on a midlatitude island. *Mon. Wea. Rev.*, 135:918–932, 2007.

J. Cuxart, J. Cunillera, M. A. Jiménez, D. Martínez, F. Molinos, and J. L. Palau. Study of mesobeta basin flows by remote sensing. *Bound.-Layer Meteor.*, 143:143–158, 2012.

F. G. DennisJr. Dormancy – what we know (and don't know). *Hort. Sci.*, 11:1249–1255, 1994.

F. G. DennisJr. Chilling requirements for the breaking of dormancy in buds of woody plants. *Hort. Sci.*, 38:347–350, 2003.

A.J. Dyer. A review of flux-profile relations. *Bound.-Layer Meteor.*, 1:363–372, 1974.

J. Egea, E. Ortega, P. Martínez-Gomez, and F. Dicenta. Chilling and heat requirements of almond cultivars for flowering. *Environmental and Experimental Botany*, 50:79–85, 2003.

F. Elías and F. Castellví. *Agrometeorología*. Mundi-Prensa Libros, 2001.

A. Erez and G. A. Couvillon. Characterization of the influence of moderate temperatures of rest completion in peach. *J. Am. Soc. Hortic. Sci.*, 112:677–680, 1987.

Estadistiques Illes Balears. Estadistiques basiques de la agricultura, la ramaderia i la pesca a les Illes Balears. Technical report, Govern de les Illes Balears, Conselleria de Presidencia, Area de Agricultura i Pesca, 2009. URL `http://www.caib.es/sacmicrofront/home.do?mkey=M72`.

S. Fishman, A. Erez, and G. A. Couvillon. The temperature-dependence of dormancy breaking in plants: computer simulation of processes studied under controlled temperatures. *J. Theor. Biol.*, 126:309–321, 1987.

Y. Fu, H. Zhang, W. Dong, and W. Yuan. Comparison of phenology models for predicting the onset of growing season over the northern hemisphere. *PLoS ONE*, 9:1–12, 2014.

R. Geiger. *The Climate near the ground*. Harvard University Press, 1965.

F. Gil-Albert. *La ecologia del arbol frutal*. Serie tecnica. M.A.P.A., Spain, 1986.

A. Ginard, A. Ordines, M.Ruiz, M. Grimalt, J. Fornós, Bernadí Gelabert, M. Laita, J. Ramon, A. Rodríguez, A. Ginés, J. Servera, and P.A. Ripoll. Atles de les Illes Balears. Technical report, Govern de les Illes Balears, Conselleria de Cultura, Educació i Esport, 1998. URL `http://www.uib.cat/secc6/lsig/Atles/INICI.HTM`.

Z. González-Parrado, C. R. Reyes Fuertes-Rodríguez, A. M. Vega-Maray, R. M. Valencia-Barrera, F. J. Rodríguez-Rajo, and D. Fernández-González. Chilling and heat requirements for the prediction of the beginning of the pollen season of Alnus glutinosa (l.) Gaertner in Ponferrada (Leon, Spain). *Aerobiologia*, 22:47–53, 2006.

M. A. Jiménez, A. Mira, J. Cuxart, A. Luque, S. Alonso, and J. A. Guijarro. Verification of a clear-sky mesoscale simulation using satellite-derived surface temperatures. *Mon. Wea. Rev.*, 136:5148–5161, 2008.

M.A. Jiménez, M.A. Cerdà, and J. Rita. The effect of the ambient conditions on the life cycle of a bulbous plant. *Tethys*, 11:39–49, 2014.

C.M. Karssen and S.P.C. Groot. The hormone-balance theory of dormancy evaluated. *British plant growth regulator group*, 15:17–30, 1987.

D.L. Liu, G. Kingston, and T.A. Bull. A new technique for determining the thermal parameters of phenological development in sugarcane, including suboptimum and supra-optimum temperature regimes. *Agricultural and Forest Meteorology*, 90:119–139, 1998.

D. Martínez and J. Cuxart. Assessment of the hydraulic slope flow approach using a mesoscale model. *Acta Geophys.*, 57:882–903, 2009.

D. Martínez, M. A. Jiménez, J. Cuxart, and L. Mahrt. Heterogeneous nocturnal cooling in a large basin under very stable conditions. *Bound.-Layer Meteor.*, 137:97–113, 2010.

F. Maselli, M. Chiesi, L. Brilli, and M. Moriondo. Simulation of olive fruit yield in Tuscany through the integration of remote sensing and ground data. *Ecological Modelling*, 244:1–12, 2012.

A. Oukabli, S. Bartolin, and R. Viti. Anatomical and morphological study of apple (Malus X domestica Borkh.) flower buds growing under inadequate winter chilling. *J. Horto. Sci. Biotech.*, 78:580–585, 2003.

D. Pope and C. Brough. *Utah's Weather and Climate*. Publishers Press, 1996.

J. R. Porter and M. Gawith. Temperatures and the growth and development of wheat: a review. *European Journal of Agronomy*, 10:23–36, 1999.

E. A. Richardson, S. D. Seeley, and D. R. Walker. A model for estimating the completion of rest for redhaven and elverta peach trees. *Hortoscience*, 4:331–332, 1974.

D. Ruiz, J. A. Campoy, and J. Egea. Chilling and heat requirements of apricot cultivars for flowering. *Environ. Exp. Bot.*, 61:254–263, 2007.

V. V. Salomonson, W. L. Bames, W. P. Maymon, and H. Montgomery. MODIS: advanced facility instrument for studies of the Earth as a system. *IEEE Trans. Geosci. Remote Sens.*, 27:145–153, 1989.

M. C. Saure. Dormancy release in deciduous fruit trees. *Horto. Rev.*, 7:239–300, 1985.

J. Schmetz, P. Pili, S. Tjemkes, D. Just, J. Kerkmann, S. Rota, and A. Ratier. An introduction to Meteosat Second Generation (MSG). *Bull. Amer. Meteor. Soc.*, 83:977–992, 2002.

M. Sharan, A.K. Yadav, M.P. Singh, P. Agarwal, and S. Nigam. A mathematical model for the dispersion of air pollutants in low wind conditions. *Atmospheric Environment*, 30: 1209–1220, 1996.

R.B. Stull. *An Introduction to Boundary Layer Meteorology.* Springer Netherlands, 1988.

M. C. Tabuenca. Chilling requirements in almond (in Spanish). *Anal. Estacion Exp. Aula Dei*, 11:325–329, 1972.

M. Teitel, U. M. Peiper, and Y. Zvieli. Shading screens for frost protection. *Agric. Forest. Meteorol*, 81:273–286, 1996.

M. Vich, M.A. Jiménez, and J. Cuxart. A study of three well-defined temporal intervals in a stably stratified night. *Tethys*, 4:33–43, 2007.

C. F. Voller. Predicting rest-breaking: principles and problems. *Deciduous Fruit Grower*, 36:302–308, 1986.

S. B. Vosper and A. R. Brown. Numerical simulations of sheltering in valleys: the formation of nighttime cold-air pools. *Bound.-Layer Meteor.*, 127:429–448, 2008.

Z. Wan and J. Dozier. A generalised split-window algorithm for retrieving land-surface temperature from space. *IEEE Trans. Geosci. Remote Sens.*, 34:892–905, 1996.